

# Robust Ultra-wideband Range Error Mitigation with Deep Learning at the Edge

Simone Angarano, Vittorio Mazzia, Francesco Salvetti, Giovanni Fantin and Marcello Chiaberge

**Abstract**—Ultra-wideband (UWB) is the state-of-the-art and most popular technology for wireless localization. Nevertheless, precise ranging and localization in non-line-of-sight (NLoS) conditions is still an open research topic. Indeed, multipath effects, reflections, refractions and complexity of the indoor radio environment can easily introduce a positive bias in the ranging measurement, resulting in highly inaccurate and unsatisfactory position estimation. This article proposes an efficient representation learning methodology that exploits the latest advancement in deep learning and graph optimization techniques to achieve effective ranging error mitigation at the edge. Channel Impulse Response (CIR) signals are directly exploited to extract high semantic features to estimate corrections in either NLoS or LoS conditions. Extensive experimentation with different settings and configurations have proved the effectiveness of our methodology and demonstrated the feasibility of a robust and low computational power UWB range error mitigation.

**Keywords**—Deep learning, Ultra-wideband, Edge AI, Indoor positioning

## I. INTRODUCTION

Precise localization is at the core of several engineering systems and due its intrinsic scientific relevance has been extensively researched in recent years [1], [2]. Either outdoor or indoor applications could largely benefit from it in fields as diverse as telecommunications [3], service robotics [4], healthcare [5], search and rescue [6] and autonomous driving [7]. Nevertheless, accurate positioning in non-line-of-sight (NLoS) conditions is still an open research problem. Multipath effects, reflections, refractions and other propagation phenomena could easily lead to error in the position estimation [8]–[10].

Ultra-wideband (UWB) is the state-of-the-art technology for wireless localization, rapidly growing in popularity [11], offering decimeter-level accuracy and increasingly smaller and cheaper transceivers [12]. With a bandwidth larger than 500 MHz and extremely short transmit pulses, UWB offers high temporal and spatial resolution and considerable multipath effect error mitigation when compared to other radio-frequency technologies [13]. Nevertheless, UWB is still primarily affected by the NLoS condition, Fig. 1, in which the range estimates based on time-of-arrival (TOA) is typically positively biased [14], [15]. That is particularly true for indoor localization where ranging errors introduced by multipath and NLoS conditions can easily achieve large deviations from the actual

position [16]. So, robust and effective mitigation is necessary to prevent large localization errors.

Several approaches have been proposed to address the NLoS problem. In the presence of a large number of anchor nodes available, NLoS identification is the preferable choice so far. Indeed, once an NLoS anchor is identified, it can be easily eliminated from the pool of nodes used for the trilateration algorithm [17]. The majority of the proposed methodologies found in the literature make use of channel and waveform statistics [18]–[20], likelihood ratio tests or binary hypothesis tests [17], [21] and machine learning techniques. In the latter case either hand-designed techniques, such as support vector machine (SVM), [22], Gaussian processes (GP), [23], or representation learning models have been investigated [8], [24].

Despite the simplicity of applying NLoS identification, [25], in almost all practical situations, there is no sufficient number of anchors available to exclude some of them. So, the majority of research community efforts focus on range and localization mitigation. As regards the latter, even if there are studies that show excellent position estimation in multipath environments, [26]–[28], the collected training data are extremely site-specific, therefore, conducting the data collection in one site does not directly allow to exploit a model in another site. On the other hand, range mitigation is far less site-specific and does not require a large amount of data to achieve satisfactory results [14]. Range error mitigation is mostly performed with similar techniques as NLoS identification [23], [29]–[31] and

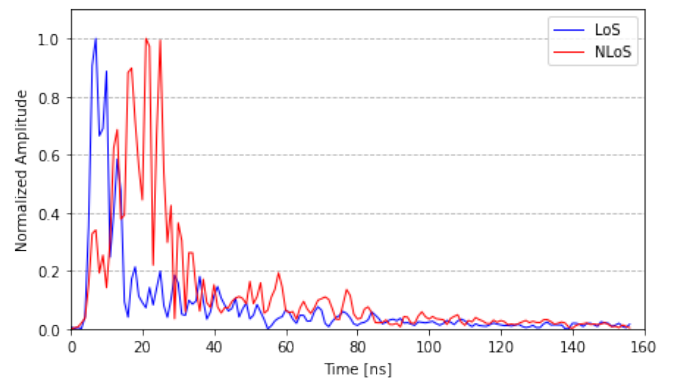


Fig. 1: LoS and NLoS CIRs with normalized amplitude in an indoor environment. In the NLoS case, the signal travels along many routes until it reaches the antenna. That makes the ToA estimation ambiguous.

The authors are with Politecnico di Torino – Department of Electronics and Telecommunications, PIC4SeR, Politecnico di Torino Interdepartmental Centre for Service Robotics and SmartData@PoliTo, Big Data and Data Science Laboratory, Italy. Email: {name.surname}@polito.it.

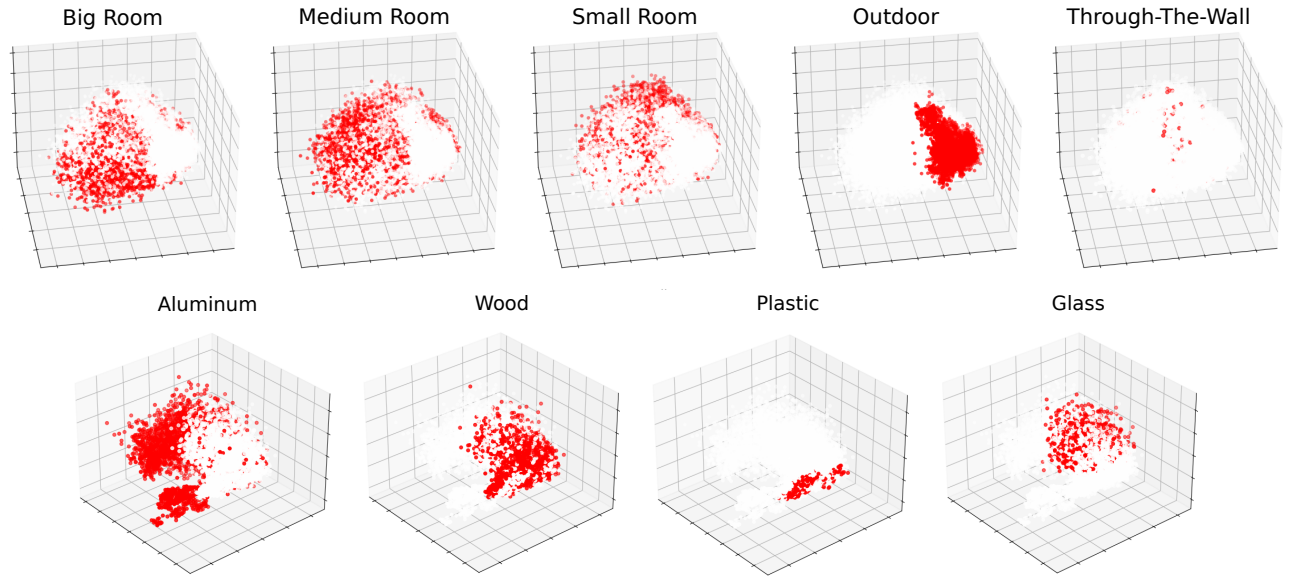


Fig. 2: Principal Component Analysis (PCA), projecting the original 157 CIR dimensions into a three-dimensional space. It is clear how rooms cover a similar data-space, completely separated by the outdoor scenario. Moreover, the same apply to materials, where more dense molecular structures affect the signal differently.

also with more extreme conditions as error mitigation for through-the-wall (TTW) [32]. Moreover, in the last few years, following the advancements brought by representation learning techniques in many fields of research [33]–[35], Bregar & Mohorčič attempted to perform range error estimation directly from the channel impulse response (CIR) using a deep learning model [36]. Nevertheless, being a preliminary study, no relevance has been given to the study of the network, optimization and capability to generalize in different environments.

This article focuses specifically on investigating a novel efficient deep learning model that performs an effective range error mitigation, making use only of the raw CIR signal, at the edge. Indeed, range error mitigation should be performed directly on board of the platform where the UWB tag is attached. So, energy consumption and computational power play a decisive role in the significant applicability of the proposed methodology. We adopt latest advancements in deep learning architectural techniques [37], [38], and graph optimization [39] to improve nearly 45% and 34% the NLoS and LoS conditions, respectively, in an unknown indoor environment up to barely 1 mJ of energy absorbed by the network during inference. Moreover, our proposed methodology does not require additional NLoS identification models but is able to extract valuable features to estimate the correct range error directly from the CIR in both LoS and NLoS states. The main contributions of this article are the following.

- 1) Design and train a highly efficient deep neural architecture for UWB range mitigation in NLoS and LoS conditions using only raw CIR data points.
- 2) Introduce weight quantization and graph optimization for power and latency reduction in range error mitigation.

- 3) Evaluate and compare several devices and hardware accelerators, annotating power and computational request for different optimized networks.
- 4) Collect and analyze a novel open-source dataset with different NLoS scenarios and settings, highlighting the generalization limitations of a hierarchical learning model.

All of our training and testing code and data are open source and publicly available<sup>1</sup>.

The rest of the paper is organized as follows. Section 2 covers the dataset creation and preliminary analyzes to assess the generalization problem of generic representation learning algorithms applied to range error mitigation. In section 3, is presented a detailed explanation of the efficient REMnet deep learning architecture and the proposed graph and quantization techniques to achieve a significant range correction for the trilateration algorithm in LoS and NLoS conditions. Finally, section 4 presents the experimental results and discussion followed by the conclusion.

## II. DATASET CONSTRUCTION

The measurements are taken in five different environments, to cover a wide variety of LoS and NLoS scenarios: an outdoor space, in which the only source of error is the presence of obstacles, and three office-like rooms, in order to include the effect of multipath components. In particular, the bigger room is approximately 10m x 5m large, the medium one is 5m x 5m and the smallest is 5m x 3.5m. Moreover, in order to analyze the TTW effect, some measurements are acquired across different rooms. Taking range measurements in

<sup>1</sup><https://zenodo.org/record/4290069#.X75qYc3-3Dc>

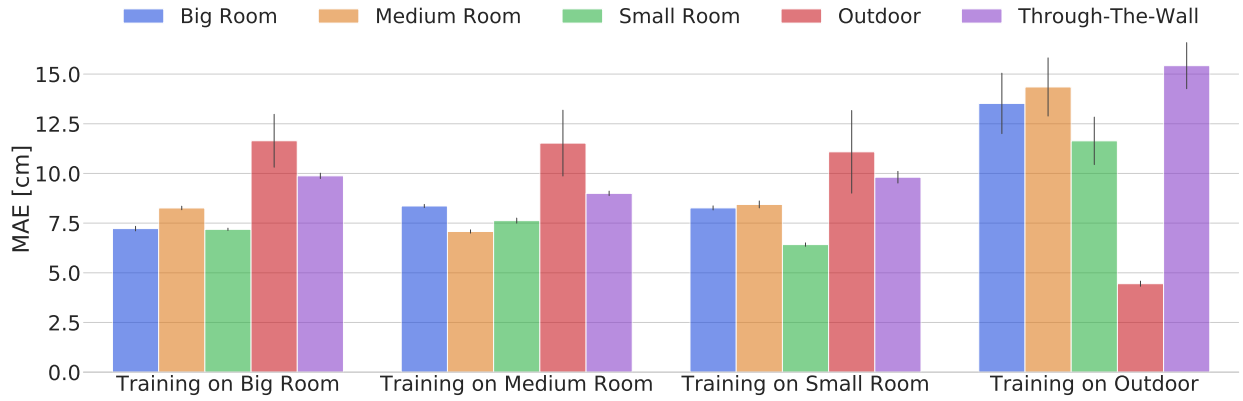


Fig. 3: Analysis of generalization capabilities in different environments of a generic representation learning model trained directly on the CIR waveform. Each bar represents an average over 20 independent MLP trainings. Results show that rooms with different sizes and configurations lead to very similar losses. Moreover, outdoor and TTW scenarios should be considered as separate settings and cannot be corrected without including appropriate samples in the training set.

different conditions also allows to perform training, validation and testing on completely different datasets, and hence avoid overfitting and encouraging a representation learning model to learn domain-independent features.

The DWM1000 boards are configured to guarantee precise ranging and high update frequency according to the constructor’s manual, and antenna delays are tuned to compensate measurement bias. The measurements are taken using a Leica AT403 laser tracker as ground truth. First, we measure the position of the anchor to have a landmark; then, the laser follows the reflector placed on the moving tag estimating its position ten times per second. Meanwhile, tag and anchor perform two-way ranging at approximately the same frequency. The tag follows a path in the environment, that is filled with obstacles to generate both LoS and NLoS measurements. After a satisfying number of samples are obtained from an environment, the configuration is changed by modifying the position of the anchor or the type and position of the obstacles.

To compute the ranging error, we match each measure with the ground-truth range coming from the laser tracker comparing timestamps. Each of the 55,000 samples of the dataset also contains the CIR vector, giving information about the transmission channel of the UWB signal. For each vector, only 152 samples after the first detected peak are retained, as suggested in [40]. Moreover, five additional samples before the peak are included to compensate for eventual errors in the detection. Finally, the environment and obstacles used for the measurements are reported to study their effect on the proposed method. As previously stated, the whole dataset is publicly released to be useful for future works on this subject [41].

#### A. Dataset analysis

In order to visualize the distribution of the acquired instances in the data space, we exploit Principal Component Analysis (PCA) to project the 157 dimensions of each CIR signal into a three-dimensional space, saving most of the original

variance. As shown in Fig. 2, in the first analysis we highlight correlations between the data points in the different analyzed environments. A prevalence of samples from the big room can be found in the lower central part of the plot, while the medium and small room samples are more present in the left and upper side of the distribution, respectively. Nevertheless, it is clear how rooms and TTW cover a similar data space, and that implies a potential transferability of statistics learnt in different indoor environments. On the other hand, the outdoor set is completely separated and wholly concentrated on the right side of the plot.

The same procedure is followed for materials, considering four object classes for clearness: aluminium plate, plastic bins, wooden door and glass. In this case, a remarkable separation is noticeable, as the metal samples occupy all the left part of the graph and light objects like plastic, wood, and glass take the right area. Moreover, the spatial distribution of wood occupies specific zones showing different features from plastic and glass. The presented qualitative analysis allows to have a first visual proof of the meaningfulness of data and draw some conclusion on how a representation learning model could perform. For example, a generic model trained on measures taken with only the presence of plastic instances would more easily mitigate the error caused by wood and less accurate estimations for metal samples.

Finally, in order to assess the generalization capabilities of a generic representation learning model trained directly on the CIR waveform, a Multilayer Perceptron (MLP) is trained and tested on different splits of the dataset. After the validity of the method is firstly verified on the whole dataset, a series of tests are conducted to study the effect of different environments and obstacles on the performance of the models. The network is trained on a specific set of data from the same environment or material and tested on the rest of the possible scenarios. In this way, it is possible to state whether the approach holds a certain generality concerning such factors. For what

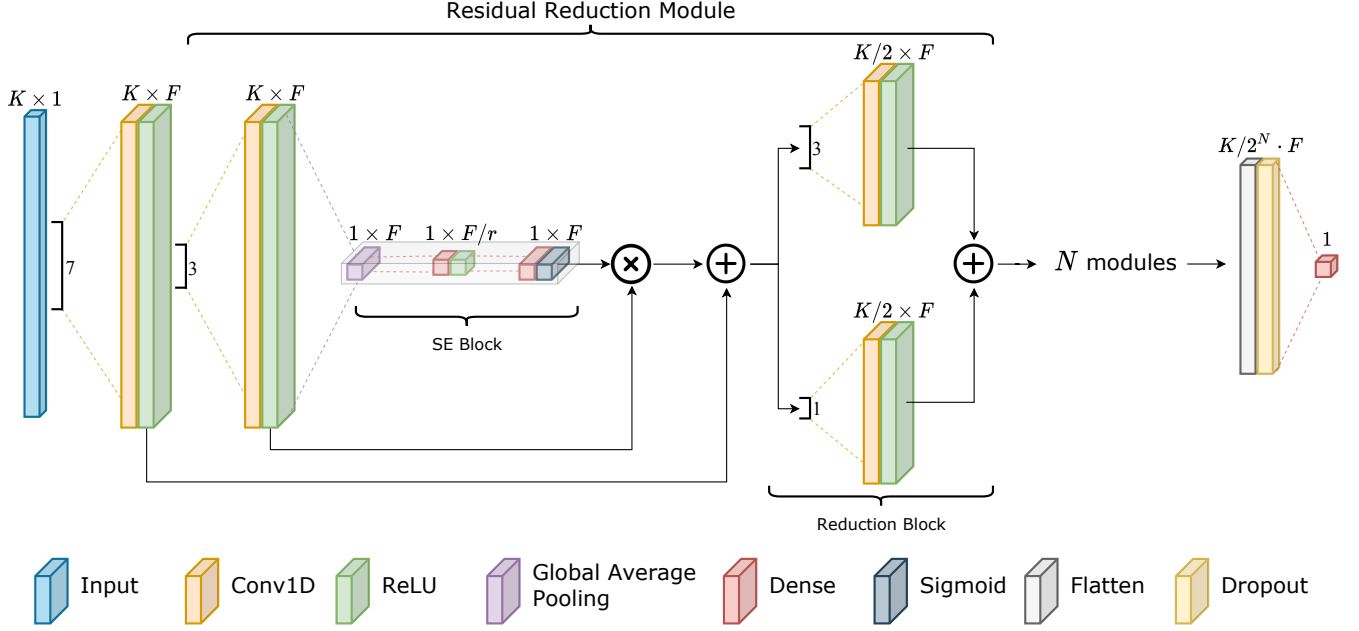


Fig. 4: Overview of the REMnet architecture. The input of the model is the  $K \times 1$  tensor representing the CIR of the measurement. The dimensionality is reduced by  $N$  subsequent Residual Reduction Modules (RRM) with a feature attention mechanism. Finally, a fully connected layer composes the high-level extracted features and outputs the range error estimation.

concerns environmental influence, resumed in Fig. 3, metrics show that rooms with different sizes and configurations lead to minimal losses (less than 2 cm) compared to those caused by outdoor measurements or more extreme conditions as TTW. Indeed, samples taken in open space show the worst results, because they are taken in a completely different scenario, and the models struggle to adapt to a situation in which multipath components are absent. Nevertheless, an improvement is achieved in almost all cases. Regarding obstacles, a more marked distinction can be noticed. As already emerged from PCA analysis, heavy materials have a very different impact on UWB signals with respect to wood, plastic and glass. However, as for different environments, there is almost always an improvement in the raw mean absolute error (MAE). That means that models are able to learn a way to compensate part of the error independently from the obstacles, and also that a dataset containing a sufficient number of examples for a wide variety of materials can lead to excellent results in many different scenarios.

### III. PROPOSED METHODOLOGY

In this section, we propose a Deep Neural Network (DNN) to solve the range error mitigation problem. Moreover, we present some optimization and quantization techniques used to increase the computational efficiency of the network. Since UWB are low-power localization devices directly connected to the mobile robot board, any error compensation technique should be applied locally on the robotic platform to ensure real-time execution with a latency compatible with the control

frequency of the robot. The method should also be as efficient as possible in order to ensure a low impact on the overall energy and computational demand of the system. In designing our solution, we mainly focus on the optimization of the model to reduce both the memory occupancy and computational efforts during inference.

#### A. Network Design

We consider the following model for a generic UWB range measurement:

$$\hat{d} = d + \Delta d$$

where the true distance  $d$  is intrinsically affected by an error  $\Delta d$  giving the final measurement outcome  $\hat{d}$ . The error depends on several factors, among which the most important is the environment and the obstacles, giving, in general, worse performance in NLoS condition.

We formulate the mitigation problem as a regression of the compensation factor  $\Delta d$  that should be added to the measured range to obtain the actual distance between the two sensors. We, therefore, design a DNN model that predicts an estimate  $\hat{y}$  for the latent true error  $y = \Delta d$  as a non-linear function of the input CIR vector  $X$ . We call the proposed architecture Range Error Mitigation network (REMNet). It is essential to underline that we do not make a distinction between LoS and NLoS measurements, but we let the network learn how to compensate both the conditions autonomously. Therefore, a classification of the measurements is not computed, but the model implicitly performs it during the mitigation process. Such an approach



allows to obtain an algorithm that is always beneficial, and that can be applied continuously on-board without the need of an additional classification step.

Due to the one-dimensional nature of the data, we select 1D convolutional layers as building blocks of the network. We denote with  $K$  the number of temporal samples low-level features with a 1D convolution. The architecture of the network is then made of a stack of  $N$  Residual Reduction Modules (RRM) that learn deep features from the high-level features while subsequently reducing the temporal dimensionality  $K$ .

The core of the RRM is composed of a residual unit with a 1D convolution followed by a Squeeze-and-Excitation block [42] on the residual branch. This block applies a feature attention mechanism by self-gating each extracted feature with a scaling factor obtained as a non-linear function of themselves. Denoting with  $f$  the  $K \times F$  tensor of feature maps extracted by the convolutional layer, we firstly squeeze it with a global average pooling layer that aggregates the tensor along the temporal dimension, obtaining a single statistic for each feature. The excitation step is then performed with a stack of one bottleneck fully connected (FC) layer that reduces the feature dimension  $F$  of a factor  $r$  and another FC layer that restores the dimensionality to  $F$  with sigmoid activation. This activation function outputs  $F$  independent scaling factors between 0 and 1 that are then multiplied with  $f$ , allowing the network to focus on the most prominent features. The residual unit is then closed summing the rescaled features with the identity branch. The residual unit is followed by a reduction block, which reduces by a factor of 2 the temporal dimension  $K$  with two parallel convolutional branches with a stride of two.

After  $N$  Residual Reduction Modules, we end up with a tensor with shape  $K/2^N \times F$ . We flatten it into a single vector, and we apply a Dropout layer to avoid overfitting and help generalization. Finally, an FC layer with linear activation computes an estimate of the compensation value  $\Delta d$ . With the exception of this final layer and the second FC layer in the SE blocks, we always apply a ReLU non-linearity to all the layers. An overview of the overall network architecture is presented in Fig. 4.

### B. Network optimization and quantization techniques

As already mentioned, a UWB range error mitigation technique should respect constraints on memory, power and latency requirements to be applicable in real-time and on-board. For this reason, we investigate different graph optimization and quantization methods to both decrease model size and computational cost. In the literature, several techniques to increase neural network efficiency can be found [39], [43]–[46]. In particular, we focus on the following main approaches:

- network pruning and layer fusing that consists in optimizing the graph by removing low-weight nodes that give almost no contribution to the outcome and fuse different operations to increase efficiency;
- weights quantization that consists of reducing the number of bits required to represent each network parameters;

- activations quantization, that reduces the representation dimension of values during the feed-forward pass, thus reducing also the computational demand;
- quantization-aware training, in which the network is trained considering a-priori the effect of quantization trying to compensate it.

We produce five different versions of REMnet, depending on the adopted techniques. The first is the plain float32 network with no modifications. To this first model, we apply graph optimization only, without quantization to investigate its effect on precision and inference efficiency. The third version is obtained by reducing the precision of the weights to 16 bits. Activations and operation still are represented as 32 bits floating points. The last two models deals instead with 8 bits full integer quantization.

This strategy is the most radical to increase network efficiency by changing the representation of both weights and activations to integers. That greatly reduce memory and computational demands due to the high efficiency of computations on integer with respect to floating-point managing. However, a great problem is how to manage completely by integer-only operations the feed-forward pass of the network. We follow the methodology presented by Jacob et al. [39] in which each weight and activation are quantized with the following scheme:

$$r = S(q - Z)$$

where  $r$  is the original floating-point value,  $q$  the integer quantized value and  $S$  and  $Z$  are the quantization parameters, respectively scale and zero point. A fixed-point multiplication approach is adopted to cope with the non-integer scale of  $S$ . Thus, all computations are performed with integer-only arithmetic making inference possible on devices that do not support floating point. We obtain two full-integer models by adopting both post-training quantization and quantization-aware training. With this second approach, fake nodes are added to the network graph, in order to simulate quantization effects during training, so that the gradient descent procedure can take into consideration the integer loss in precision.

All the inference results obtained with the five models are presented in Section IV-B.

## IV. EXPERIMENTS AND RESULTS

In this section, we perform an experimental evaluation of the proposed neural efficient architecture for range error mitigation. Moreover, we test the accuracy and performance of different optimized versions of the network on disparate heterogeneous devices collecting energy and computational requirements.

### A. Experimental setting

In the following experiments, we employ the presented dataset of Section II keeping aside the medium size room as the testing set. Indeed, instead of performing a stratified sampling of the available data, in the light of the evidence of Section II-A, we decide to perform all tests with indoor instances. That is more similar to an actual infield application and

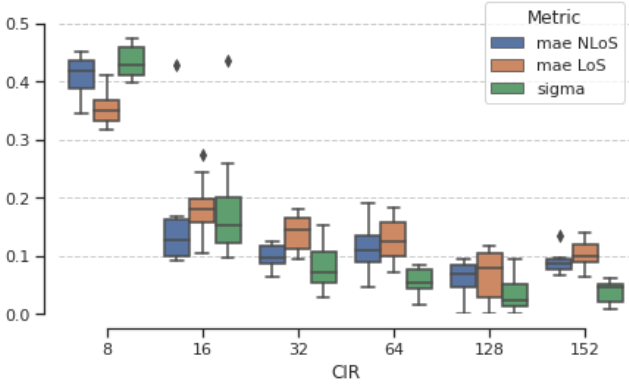


Fig. 5: Network performances with different CIR sizes  $K$ , starting from the dimension suggested by [36]. Progressively training with a reduced number of input features degrades the performance of the network. An input with eight dimensions appears to be the minimum required to obtain an acceptable range error estimation.

better highlights the generalization capabilities of the proposed methodology. So, all experimentations are performed with 36023 and 13210 training and testing data points, respectively, keeping aside TTW and outdoor measurements. Finally, due to their very different nature, and explicitly labelled LoS samples are employed to evaluate the capability of the network to recognize this condition and act accordingly.

The final test consists in using the best-developed model for a 3D positioning task in order to assess the effect of range mitigation on localization accuracy. The medium room is chosen as the testing environment, as its samples have not been used to train the networks. Four UWB anchors are placed in the room, and a fixed tag is put in the centre. First, the laser tracker precisely measures the positions of all the nodes to provide ground truth, then the acquisition of the data begins. Two situations are taken into consideration, a fully LoS scenario and a critical NLoS one. Once the samples have been collected, they are prepared for the processing phase, in which the range measurements are used to estimate the 3D position of the tag employing a simple Gauss-Newton non-linear optimization algorithm.

All network hyperparameters are obtained with an initial random search analysis followed by a grid search exploration to fine-tune them and find a compromise between accuracy and efficiency. Indeed, working at the architecture level is crucial to satisfy the constraints given by the studied application. The number of filters,  $F$ , is equal to 16 and the number of reduction module  $N = 3$  with  $r = 8$ . As shown in Fig. 4, all 1D convolutional operations have a kernel of size 3, with the exception of the first layer and the second branch of the reduction block. The resulting network has an efficient and highly optimized architecture with 6151 trainable parameters. Finally, in order to select the optimal number of input features, as shown in Fig. 5, we progressively reduced the input number of dimensions  $K$  while annotating the metrics of the network.

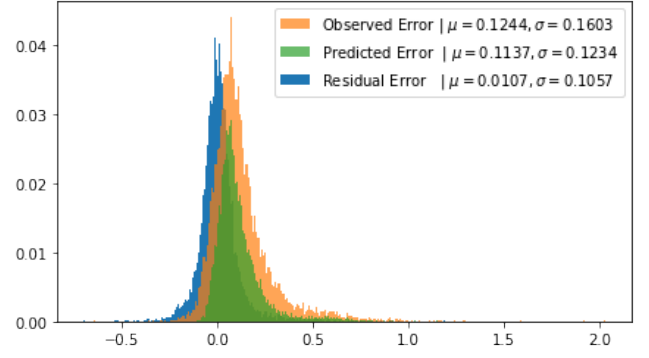


Fig. 6: Normalized histograms with 300 bins each. It is possible to notice how the residual range error distribution (blue histogram) is almost Gaussian. That greatly improves the optimality and simplicity of the subsequent iterative localization algorithm [49].

All points are the average result of ten consecutive trials. Experimentation shows that eight dimensions are the minimum number of features required to the network to obtain an acceptable range error estimation. Moreover, we empirically find that an input CIR of 152 elements, as suggested by [36], is redundant and could even slightly reduce the performance of the model. On the other hand, fewer dimensions of 128 tend almost linearly to degrade the accuracy of the network.

The Adam optimization algorithm [47] is employed for training, with momentum parameters  $\beta_1 = 0.9$ ,  $\beta_2 = 0.999$ , and  $\epsilon = 10^{-8}$ . The optimal learning rate,  $\eta = 3e - 4$ , is experimentally derived using the methodology described in [48]. That is kept constant for 30 epochs with a batch size of 32 and MAE as the loss function. We employ the TensorFlow framework to train the network on a PC with 32-GB RAM and an Nvidia 2080 Super GP-GPU. The overall training process can be performed in less than 10 minutes.

### B. Quantitative results

The data samples of the medium room have a starting MAE of 0.1242 m and a standard deviation of  $\sigma = 0.1642$  m. On the other hand, the starting MAE of explicitly labelled LoS samples is of 0.0594 m.

In Fig. 6 are shown the results obtained by the reference architecture trained with the setting illustrated in subsection IV-A. It is possible to notice how the network is able to almost completely compensate the offset of the original range error and reduce the standard deviation of 34.1%. Moreover, as summarized in Table I, the network can easily detect LoS input signals and apply a small correction factor that takes into account the multipath effect. That is proved by the residual error MAE that has a percentage improvement of 25.1%. On the other hand, MAE for NLoS signals is improved of 44.7%, reducing the error to 0.0697 m that is near the actual precision of DWM1000 boards [50].

Finally, in Table I are also shown three baseline approaches as a comparison. For support vector machine (SVM) and MLP,

|                                    | MAE [NLoS] | MAE [LoS] | $R^2$ [NLoS] | $R^2$ [LoS] | $\sigma$ [NLoS] |
|------------------------------------|------------|-----------|--------------|-------------|-----------------|
| Support Vector Machine (SVM)       | 0,0766     | 0,0507    | 0,4444       | 0,1256      | 0,1171          |
| Multilayer Perceptron (MLP)        | 0,0796     | 0,0466    | 0,4194       | 0,2913      | 0,1170          |
| CNN-1D [36]                        | 0,0890     | 0,0523    | 0,2870       | 0,1089      | 0,1285          |
| REMnet float32                     | 0,0687     | 0,0445    | 0,5607       | 0,3483      | 0,1057          |
| Graph Optimization                 | 0,0687     | 0,0445    | 0,5607       | 0,3483      | 0,1057          |
| Post-training float16 quantization | 0,0688     | 0,0445    | 0,5607       | 0,3484      | 0,1058          |
| Post-training 8-bit quantization   | 0,0712     | 0,0455    | 0,5361       | 0,3100      | 0,1082          |
| Full-integer aware quantization    | 0,0708     | 0,0449    | 0,5404       | 0,3357      | 0,1079          |

TABLE I: Proposed architecture performances after graph optimization and different levels of weight quantization. Initial values of MAE for NLoS and LoS signals are 0.1242 m and 0.0594, respectively. It is possible to notice how the different transformations barely affect the range error estimation capability of the network. Moreover, three baseline approaches are tested and compared with the efficient REMnet model and its optimization versions.

we adopt the six hand-crafted features described in [18], [51]. We use radial basis function as the kernel for our SVM and a 3-layer architecture with 64 hidden neurons for the MLP. Instead, for [36], we feed the network with 152 bins, and we set the hyperparameters suggested in the article. It is noticeable how REMnet, even with a highly efficient architecture, has better performances of other literature methodologies.

1) *Power and latency optimization*: Range error mitigation should be performed directly on board of the platform where the UWB tag is attached. So, energy consumption and computational power play a decisive role in the effective applicability of the proposed methodology. However, real-time range mitigation with the whole CIR could be very computational intensive [52]. Consequently, in order to comply with cost, energy, size and computational constraints, instead of manually extracting a reduced number of features from the CIR, we investigate effects of optimization, detailed in section III, on the accuracy of the network.

Graph optimization techniques and different level of weights quantization are both examined, starting from the pre-trained reference network. In Table I are summarized the performances of the model after different optimization processes. Even if there is a degradation of the overall metrics, these changes are mostly negligible. Moreover, it is possible to notice that the full-integer quantization, which generally produces a size reduction and speed-up of 75%, if carried out with an awareness training, it decreases the NLoS MAE only of the 3%. That opens the possibility to achieve effective range mitigation with an almost negligible impact on the overall application. Indeed, a so extreme weight quantization implies a smaller model size with less memory usage, an important latency reduction and the possibility to use highly efficient neural accelerators.

2) *Inference results*: In this section, we test different optimized networks on several devices and hardware accelerators, annotating power and computational request. The choice for the selected microchips is made performing a market evaluation at the time of writing that takes into consideration common computational boards for indoor navigation. Indeed, robotic platforms are usually endowed with a Linux-capable Arm Cortex-A CPUs or powerful co-processors and accelerators as Nvidia GP-GPUs, Visual Processing Units (VPUs) or Tensor

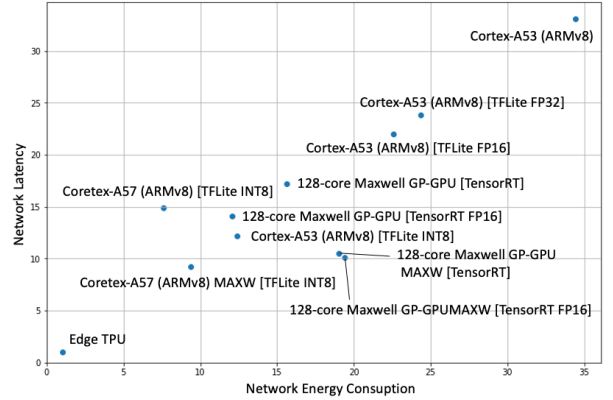


Fig. 7: Energy and latency are two important constraints for an effective range error mitigation. Indeed, error correction is performed progressively over all received anchor signals on board of the platform connected with the tag. Without an highly optimized and efficient correction model, range error mitigation would not be applicable.

Processing Units (TPUs). We adopt two standard libraries for networks deployment, TensorFlow-Lite<sup>2</sup> and TensorRT<sup>3</sup> to produce the optimized networks. Both are directly integrated into the TensorFlow framework and are specifically conceived to target different hardware platforms. In particular, we target Cortex-A53, A57 processors and Edge TPU with TF-Lite and the Nvidia RTX 2080 and 128-core Maxwell GP-GPUs with TensorRT.

Experimentation results are summarized in Table II. It is possible to notice that, due to the high efficiency of the proposed architecture, all configurations satisfy a sufficient inference speed compliant for an effective range error mitigation solution. Nevertheless, the different optimization techniques applied have a high impact factor on the energy consumed by the network. Indeed, considering experimentations performed

<sup>2</sup><https://www.tensorflow.org/lite>

<sup>3</sup><https://developer.nvidia.com/tensorrt>

| Device           | G.O. | W.P. | Latency [ms] | Latency <sub>4 batch</sub> [ms] | V <sub>al</sub> [V] | I <sub>idl</sub> [A] | P <sub>run</sub> [W] | E <sub>net</sub> [mJ] | Size [KB] |
|------------------|------|------|--------------|---------------------------------|---------------------|----------------------|----------------------|-----------------------|-----------|
| RTX 2080         | N    | FP32 | 19.7 ± 0.23  | 19.3 ± 0.24                     | N.A.                | N.A.                 | 32                   | 617.6                 | 250.0     |
|                  | Y    | FP32 | 0.69 ± 0.13  | 0.69 ± 0.16                     | N.A.                | N.A.                 | 20                   | 138.0                 | 613.0     |
|                  | Y    | FP16 | 0.54 ± 0.09  | 0.51 ± 0.02                     | N.A.                | N.A.                 | 18                   | 97.2                  | 615.0     |
| Cortex-A53       | N    | FP32 | 16.9 ± 0.03  | 17.2 ± 0.05                     | 5.0                 | 0.4                  | 1.0                  | 17.2                  | 250.0     |
|                  | Y    | FP32 | 12.2 ± 0.03  | N.A.                            | 5.0                 | 0.4                  | 1.0                  | 12.2                  | 40.7      |
|                  | Y    | FP16 | 11.2 ± 0.03  | N.A.                            | 5.0                 | 0.4                  | 1.0                  | 11.2                  | 33.9      |
|                  | Y    | INT8 | 6.23 ± 0.02  | N.A.                            | 5.0                 | 0.4                  | 1.0                  | 6.2                   | 32.7      |
| Cortex-A57       | Y    | INT8 | 7.63         | N.A.                            | 5.0                 | 0.5                  | 0.8                  | 3.81                  | 32.7      |
|                  | Y    | INT8 | 4.71         | N.A.                            | 5.0                 | 0.5                  | 1.0                  | 4.7                   | 32.7      |
|                  | Y    | FP32 | 8.78 ± 0.09  | 9.03 ± 0.1                      | 5.0                 | 0.67                 | 0.9                  | 7.8                   | 615.0     |
| 128-core Maxwell | Y    | FP16 | 7.22 ± 0.08  | 7.43 ± 0.05                     | 5.0                 | 0.67                 | 0.9                  | 6.04                  | 613.0     |
|                  | Y    | FP32 | 5.36 ± 0.05  | 5.29 ± 0.05                     | 5.0                 | 0.5                  | 1.8                  | 9.7                   | 615.0     |
|                  | Y    | FP16 | 5.18 ± 0.04  | 5.39 ± 0.05                     | 5.0                 | 0.5                  | 1.0                  | 4.7                   | 613.0     |
|                  | Y    | INT8 | 0.51 ± 0.1   | N.A.                            | 5.0                 | 0.59                 | 0.7                  | 0.5                   | 70.54     |

TABLE II: Comparison between different devices energy consumption and inference performances. Graph optimization (G.O.) and weight precision (W.P.) reduction further increase the capability of our already efficient neural network design helping to deal with energy, speed, size and cost constraints.

with the Cortex-A53, optimization can reduce the energy consumption by nearly a factor of three, starting with an initial value of 17.2 mJ to barely 6.2 mJ with a reduction of 64%. Moreover, the model size is greatly reduced from 250 KB to 32.7 KB. That implies smaller storage size and less RAM at run-time, freeing up memory for the main application where UWB localization is needed. Finally, as further highlighted by Fig. 7 and the results of the previous subsection, the Edge TPU neural accelerator with a full-integer quantized aware training model is the preferable solution for deployment. With only a latency of 0.51 ms and energy consumption of 0.5 mJ, it barely impacts the performance of the overall application and allows to exploit duty cycling and energy-saving techniques. Indeed, as stated by our proposed methodology section, the already efficient design of our architecture, in conjunction with 8-bit weight precision and graph optimization techniques, makes deep learning a feasible solution for an effective range error mitigation for UWB at the edge.

3) *Trilateration results:* As described in IV-A, the effect of the proposed method is lastly verified by using the model featuring full-integer aware quantization for a 3D positioning task, in which the results obtained from raw range estimates and the ones achieved inserting our mitigation model in the process are compared. The results are summarized in Table III, while Fig. 8 gives a graphical representation of the NLoS results. As regards the LoS case, the positioning system already achieves a good precision by itself with very low range MAE and, consequently, a low position MAE. As a matter of fact, the effect of mitigation is irrelevant, causing a slight increment of ranging error but a slight decrease in positioning error. So, as expected, the model learns to apply very slight corrections to LoS samples, avoiding to worsen already good measurements. The NLoS scenario, instead, shows a significant improvement, as the range MAE is more than halved, reaching a value that is comparable to the LoS case and confirming the results shown in IV-B. As a consequence, the error on the position estimation is strongly reduced, going from 57.7 cm to 18.2 cm. Although

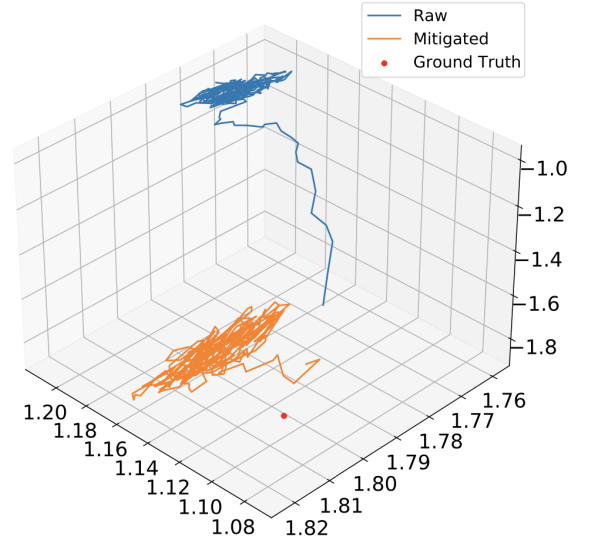


Fig. 8: Comparison between position estimations of a fixed tag in NLoS conditions. In light blue the results obtained from raw range measurements, in orange the ones achieved with our quantization aware mitigation model.

the final accuracy is still significantly higher than the one found in the LoS case, a reduction of 68% is to be considered an important result. Indeed, our approach allows achieving a precision that is suitable for many kinds of indoor robotic applications showing a very good generalization to unknown environments.

## V. CONCLUSIONS

We introduced REMnet, a novel representation learning model accurately designed to constitute an effective range error mitigation solution. Moreover, we proposed a set of



|                                 | LOS           |                  | NLOS          |                  |
|---------------------------------|---------------|------------------|---------------|------------------|
|                                 | Range MAE [m] | Position MAE [m] | Range MAE [m] | Position MAE [m] |
| Raw UWB Measurements            | 0.0388        | 0.0703           | 0.1129        | 0.5772           |
| Full-integer Aware Quantization | 0.0465        | 0.0679           | 0.0571        | 0.1817           |

TABLE III: Results obtained from the positioning test in the medium room, that is not used for the training of the model. For each test, the mean absolute error is reported for both the range estimates and the final position result, in order to highlight the effect of the former on the latter.

optimization techniques to enhance its efficiency and computational results further. Extensive experimentation proved the effectiveness of our methodology and generality over disparate scenarios. Further works will aim at integrating the deep learning architecture on an ultra-low-power microcontroller directly placed on the UWB device.

#### ACKNOWLEDGEMENTS

This work has been developed with the contribution of the Politecnico di Torino Interdepartmental Centre for Service Robotics PIC4SeR<sup>4</sup> and SmartData@Polito<sup>5</sup>. Moreover, it is partially supported by the Italian government via the NG-UWB project (MIUR PRIN 2017).

#### REFERENCES

- [1] F. Zafari, A. Gkelias, and K. K. Leung, "A survey of indoor localization systems and technologies," *IEEE Communications Surveys & Tutorials*, vol. 21, no. 3, pp. 2568–2599, 2019.
- [2] Q. D. Vo and P. De, "A survey of fingerprint-based outdoor localization," *IEEE Communications Surveys & Tutorials*, vol. 18, no. 1, pp. 491–506, 2015.
- [3] E. Y. Menta, N. Malm, R. Jäntti, K. Ruttki, M. Costa, and K. Leppänen, "On the performance of aoa-based localization in 5g ultra-dense networks," *IEEE Access*, vol. 7, pp. 33 870–33 880, 2019.
- [4] N. Karlsson, M. E. Munich, L. Goncalves, J. Ostrowski, E. Di Bernardo, and P. Pirjanian, "Core technologies for service robotics," in *2004 IEEE/RSJ International Conference on Intelligent Robots and Systems (IROS)(IEEE Cat. No. 04CH37566)*, vol. 3. IEEE, 2004, pp. 2979–2984.
- [5] B. Cheng, L. Cui, W. Jia, W. Zhao, and P. H. Gerhard, "Multiple region of interest coverage in camera sensor networks for tele-intensive care units," *IEEE Transactions on Industrial Informatics*, vol. 12, no. 6, pp. 2331–2341, 2016.
- [6] S. Zorn, R. Rose, A. Goetz, and R. Weigel, "A novel technique for mobile phone localization for search and rescue applications," in *2010 International Conference on Indoor Positioning and Indoor Navigation*. IEEE, 2010, pp. 1–4.
- [7] K. Jo, K. Chu, and M. Sunwoo, "Gps-bias correction for precise localization of autonomous vehicles," in *2013 IEEE Intelligent Vehicles Symposium (IV)*. IEEE, 2013, pp. 636–641.
- [8] M. Stahlke, S. Kram, C. Mutschler, and T. Mahr, "Nlos detection using uwb channel impulse responses and convolutional neural networks," in *2020 International Conference on Localization and GNSS (ICL-GNSS)*. IEEE, 2020, pp. 1–6.
- [9] W. Wen, G. Zhang, and L.-T. Hsu, "Gnss nlos exclusion based on dynamic object detection using lidar point cloud," *IEEE Transactions on Intelligent Transportation Systems*, 2019.
- [10] J. Ray, J. Griffiths, X. Collilieux, and P. Rebischung, "Subseasonal gnss positioning errors," *Geophysical Research Letters*, vol. 40, no. 22, pp. 5854–5860, 2013.
- [11] P. Tiwari and P. K. Malik, "Design of uwb antenna for the 5g mobile communication applications: A review," in *2020 International Conference on Computation, Automation and Knowledge Management (ICCAKM)*. IEEE, 2020, pp. 24–30.
- [12] V. Magnago, P. Corbalán, G. P. Picco, L. Palopoli, and D. Fontanelli, "Robot localization via odometry-assisted ultra-wideband ranging with stochastic guarantees," in *IROS*, 2019, pp. 1607–1613.
- [13] L. Schmid, D. Salido-Monzú, and A. Wieser, "Accuracy assessment and learned error mitigation of uwb tof ranging," in *2019 International Conference on Indoor Positioning and Indoor Navigation (IPIN)*. IEEE, 2019, pp. 1–8.
- [14] V. Savic, E. G. Larsson, J. Ferrer-Coll, and P. Stenumgaard, "Kernel methods for accurate uwb-based ranging with reduced complexity," *IEEE Transactions on Wireless Communications*, vol. 15, no. 3, pp. 1783–1793, 2015.
- [15] T. Otim, L. E. Díez, A. Bahillo, P. Lopez-Iturri, and F. Falcone, "Effects of the body wearable sensor position on the uwb localization accuracy," *Electronics*, vol. 8, no. 11, p. 1351, 2019.
- [16] Y.-Y. Chen, S.-P. Huang, T.-W. Wu, W.-T. Tsai, C.-Y. Liou, and S.-G. Mao, "Uwb system for indoor positioning and tracking with arbitrary target orientation, optimal anchor location, and adaptive nlos mitigation," *IEEE Transactions on Vehicular Technology*, 2020.
- [17] B. Silva and G. P. Hancke, "Ir-uw-b-based non-line-of-sight identification in harsh environments: Principles and challenges," *IEEE Transactions on Industrial Informatics*, vol. 12, no. 3, pp. 1188–1195, 2016.
- [18] S. Marano, W. M. Gifford, H. Wymeersch, and M. Z. Win, "Nlos identification and mitigation for localization based on uwb experimental data," *IEEE Journal on selected areas in communications*, vol. 28, no. 7, pp. 1026–1035, 2010.
- [19] J. Schroeder, S. Galler, K. Kyamakya, and K. Jobmann, "Nlos detection algorithms for ultra-wideband localization," in *2007 4th Workshop on Positioning, Navigation and Communication*. IEEE, 2007, pp. 159–166.
- [20] V. Barral, C. J. Escudero, and J. A. García-Naya, "Nlos classification based on rss and ranging statistics obtained from low-cost uwb devices," in *2019 27th European Signal Processing Conference (EUSIPCO)*. IEEE, 2019, pp. 1–5.
- [21] A. H. Muqaibel, M. A. Landolsi, and M. N. Mahmood, "Practical evaluation of nlos/los parametric classification in uwb channels," in *2013 1st International Conference on Communications, Signal Processing, and their Applications (ICCSPA)*. IEEE, 2013, pp. 1–6.
- [22] R. Ying, T. Jiang, and Z. Xing, "Classification of transmission environment in uwb communication using a support vector machine," in *2012 IEEE Globecom Workshops*. IEEE, 2012, pp. 1389–1393.
- [23] Z. Xiao, H. Wen, A. Markham, N. Trigoni, P. Blunsom, and J. Frolik, "Non-line-of-sight identification and mitigation using received signal strength," *IEEE Transactions on Wireless Communications*, vol. 14, no. 3, pp. 1689–1702, 2014.
- [24] C. Jiang, J. Shen, S. Chen, Y. Chen, D. Liu, and Y. Bo, "Uwb nlos/los

<sup>4</sup><https://pic4ser.polito.it>

<sup>5</sup><https://smartdata.polito.it>

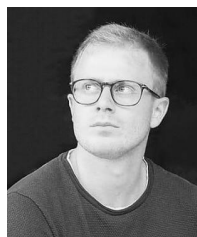
- classification using deep learning method,” *IEEE Communications Letters*, vol. 24, no. 10, pp. 2226–2230, 2020.
- [25] K. Gururaj, A. K. Rajendra, Y. Song, C. L. Law, and G. Cai, “Real-time identification of nlos range measurements for enhanced uwb localization,” in *2017 International Conference on Indoor Positioning and Indoor Navigation (IPIN)*. IEEE, 2017, pp. 1–7.
- [26] A. Niitsoo, T. Edelh  ber, and C. Mutschler, “Convolutional neural networks for position estimation in tdoa-based locating systems,” in *2018 International Conference on Indoor Positioning and Indoor Navigation (IPIN)*. IEEE, 2018, pp. 1–8.
- [27] C.-H. Hsieh, J.-Y. Chen, and B.-H. Nien, “Deep learning-based indoor localization using received signal strength and channel state information,” *IEEE access*, vol. 7, pp. 33 256–33 267, 2019.
- [28] A. Poullose and D. S. Han, “Uwb indoor localization using deep learning lstm networks,” *Applied Sciences*, vol. 10, no. 18, p. 6290, 2020.
- [29] Z. Zeng, R. Bai, L. Wang, and S. Liu, “Nlos identification and mitigation based on cir with particle filter,” in *2019 IEEE Wireless Communications and Networking Conference (WCNC)*. IEEE, 2019, pp. 1–6.
- [30] C. Mao, K. Lin, T. Yu, and Y. Shen, “A probabilistic learning approach to uwb ranging error mitigation,” in *2018 IEEE Global Communications Conference (GLOBECOM)*. IEEE, 2018, pp. 1–6.
- [31] H. Wymeersch, S. Marano, W. M. Gifford, and M. Z. Win, “A machine learning approach to ranging error mitigation for uwb localization,” *IEEE transactions on communications*, vol. 60, no. 6, pp. 1719–1728, 2012.
- [32] B. J. Silva and G. P. Hancke, “Ranging error mitigation for through-the-wall non-line-of-sight conditions,” *IEEE Transactions on Industrial Informatics*, 2020.
- [33] A. Khaliq, V. Mazzia, and M. Chiaberge, “Refining satellite imagery by using uav imagery for vineyard environment: A cnn based approach,” in *2019 IEEE International Workshop on Metrology for Agriculture and Forestry (MetroAgriFor)*. IEEE, 2019, pp. 25–29.
- [34] D. Aghi, V. Mazzia, and M. Chiaberge, “Local motion planner for autonomous navigation in vineyards with a rgb-d camera-based algorithm and deep learning synergy,” *Machines*, vol. 8, no. 2, p. 27, 2020.
- [35] F. Salvetti, V. Mazzia, A. Khaliq, and M. Chiaberge, “Multi-image super resolution of remotely sensed images using residual attention deep neural networks,” *Remote Sensing*, vol. 12, no. 14, p. 2207, 2020.
- [36] K. Bregar and M. Mohor  i , “Improving indoor localization using convolutional neural networks on computationally restricted devices,” *IEEE Access*, vol. 6, pp. 17 429–17 441, 2018.
- [37] W. Wang and J. Shen, “Deep visual attention prediction,” *IEEE Transactions on Image Processing*, vol. 27, no. 5, pp. 2368–2378, 2017.
- [38] C. Szegedy, S. Ioffe, V. Vanhoucke, and A. Alemi, “Inception-v4, inception-resnet and the impact of residual connections on learning,” *arXiv preprint arXiv:1602.07261*, 2016.
- [39] B. Jacob, S. Kligys, B. Chen, M. Zhu, M. Tang, A. Howard, H. Adam, and D. Kalenichenko, “Quantization and training of neural networks for efficient integer-arithmetic-only inference,” in *Proceedings of the IEEE Conference on Computer Vision and Pattern Recognition*, 2018, pp. 2704–2713.
- [40] K. Bregar and M. Mohorcic, “Improving Indoor Localization Using Convolutional Neural Networks on Computationally Restricted Devices,” *IEEE Access*, vol. 6, pp. 17 429–17 441, 2018.
- [41] S. Angarano, F. Salvetti, V. Mazzia, G. Fantin, and M. Chiaberge, “Deep UWB: A dataset for UWB ranging error mitigation in indoor environments.” [Online]. Available: <https://zenodo.org/record/4290069#.X75qYc3-3Dc>
- [42] J. Hu, L. Shen, and G. Sun, “Squeeze-and-excitation networks,” in *Proceedings of the IEEE conference on computer vision and pattern recognition*, 2018, pp. 7132–7141.
- [43] Y. Gong, L. Liu, M. Yang, and L. Bourdev, “Compressing deep convolutional networks using vector quantization,” *arXiv preprint arXiv:1412.6115*, 2014.
- [44] S. Gupta, A. Agrawal, K. Gopalakrishnan, and P. Narayanan, “Deep learning with limited numerical precision,” in *International Conference on Machine Learning*, 2015, pp. 1737–1746.
- [45] S. Han, X. Liu, H. Mao, J. Pu, A. Pedram, M. A. Horowitz, and W. J. Dally, “Eie: efficient inference engine on compressed deep neural network,” *ACM SIGARCH Computer Architecture News*, vol. 44, no. 3, pp. 243–254, 2016.
- [46] S. Han, H. Mao, and W. J. Dally, “Deep compression: Compressing deep neural networks with pruning, trained quantization and huffman coding,” *arXiv preprint arXiv:1510.00149*, 2015.
- [47] D. P. Kingma and J. Ba, “Adam: A method for stochastic optimization,” *arXiv preprint arXiv:1412.6980*, 2014.
- [48] L. N. Smith, “Cyclical learning rates for training neural networks,” in *2017 IEEE Winter Conference on Applications of Computer Vision (WACV)*. IEEE, 2017, pp. 464–472.
- [49] S. S  rkk  , *Bayesian filtering and smoothing*. Cambridge University Press, 2013, vol. 3.
- [50] A. R. Jim  nez and F. Seco, “Comparing decawave and bespoon uwb location systems: Indoor/outdoor performance analysis,” in *2016 International Conference on Indoor Positioning and Indoor Navigation (IPIN)*. IEEE, 2016, pp. 1–8.
- [51] S. Mazuelas, A. Conti, J. C. Allen, and M. Z. Win, “Soft range information for network localization,” *IEEE Transactions on Signal Processing*, vol. 66, no. 12, pp. 3155–3168, 2018.
- [52] Z. Zeng, S. Liu, and L. Wang, “Nlos identification for uwb based on channel impulse response,” in *2018 12th International Conference on Signal Processing and Communication Systems (ICSPCS)*. IEEE, 2018, pp. 1–6.



**Simone Angarano** is a research fellow at PIC4SeR (<https://pic4ser.polito.it/>). He achieved a Bachelor's Degree in Electronic Engineering in 2018 and a Master's Degree in Mechatronics Engineering in 2020 at Politecnico di Torino, presenting the thesis "Deep Learning Methodologies for UWB Ranging Error Compensation". His research focuses on Machine Learning for robotic applications in everyday-life contexts.



**Marcello Chiaberge** is currently Associate Professor within the Department of Electronics and Telecommunications, Politecnico di Torino, Turin, Italy. He is also the Co-Director of the Mechatronics Lab, Politecnico di Torino ([www.lim.polito.it](http://www.lim.polito.it)), Turin, and the Director and the Principal Investigator of the new Centre for Service Robotics (PIC4SeR, <https://pic4ser.polito.it/>), Turin. He has authored more than 100 articles accepted in international conferences and journals, and he is the coauthor of nine international patents. His research interests include hardware implementation of neural networks and fuzzy systems and the design and implementation of reconfigurable real-time computing architectures.



**Vittorio Mazzia** is a Ph.D. student in Electrical, Electronics and Communications Engineering working with the two Interdepartmental Centres PIC4SeR (<https://pic4ser.polito.it/>) and SmartData (<https://smartdata.polito.it/>). He received a master's degree in Mechatronics Engineering from the Politecnico di Torino, presenting a thesis entitled "Use of deep learning for automatic low-cost detection of cracks in tunnels," developed in collaboration with the California State University. His current research interests involve deep learning applied to different

tasks of computer vision, autonomous navigation for service robotics, and reinforcement learning. Moreover, making use of neural compute devices (like Jetson Xavier, Jetson Nano, Movidius Neural Stick) for hardware acceleration, he is currently working on machine learning algorithms and their embedded implementation for AI at the edge.



**Francesco Salvetti** is currently a Ph.D. student in Electrical, Electronics and Communications Engineering in collaboration with the two interdepartmental centers PIC4SeR (<https://pic4ser.polito.it/>) and Smart Data (<https://smartdata.polito.it/>) at Politecnico di Torino, Italy. He received his Bachelor's Degree in Electronic Engineering in 2017 and his Master's Degree in Mechatronics Engineering in 2019 at Politecnico di Torino. He is currently working on Machine Learning applied to Computer Vision and Image Processing in robotics applications.



**Giovanni Fantin** is a research fellow at PIC4SeR (<https://pic4ser.polito.it/>). In 2019, he achieved the Master's Degree in Mechatronics Engineering at Politecnico di Torino discussing the thesis "UWB localization system for partially GPS denied robotic applications". He is currently working on a PRIN (progetto di rilevante interesse nazionale) about new generation ultra-wideband technologies with a particular focus on multi-robot cooperation to perform localization.